Interplay between beam-driven chirping modes and plasma confinement transitions in spherical tokamak ST40

OPEN ACCESS
IOP Publishing | International Atomic Energy Agency
Nuclear Fusion
Nucl. Fusion **63** (2023) 016024 (8pp)
https://doi.org/10.1088/1741-4326/aca54d

Interplay between beam-driven chirping modes and plasma confinement transitions in spherical tokamak ST40

J. Bland[1,*], J. Varje[1], N.N. Gorelenkov[2], M.P. Gryaznevich[1], S.E. Sharapov[3], J. Wood[1] and The ST40 Team[1]

[1] Tokamak Energy Ltd, 173 Brook Drive, Milton Park, Oxfordshire, OX14 4SD, United Kingdom of Great Britain and Northern Ireland
[2] PPPL, 100 Stellarator Rd, Princeton, NJ, 08540, United States of America
[3] CCFE, Culham Science Centre, Abingdon, Oxfordshire OX14 3DB, United Kingdom of Great Britain and Northern Ireland

E-mail: james.bland@tokamakenergy.co.uk

Received 2 August 2022, revised 25 October 2022
Accepted for publication 23 November 2022
Published 14 December 2022

Abstract

Experiments on the high field spherical tokamak ST40 have led to the recent observation of interplay between beam-driven modes of sweeping frequency (chirping modes) and transitions to the enhanced global confinement regime (H-mode) and back to the low confinement regime (L-mode). The H-modes of plasma confinement are identified from decreased intensity of D_α signal and from clear distinctions in the edge gradients of the visible plasma boundary (observed as a sharp plasma edge in camera images). The beam-driven chirping modes, identified as ideal magnetohydrodynamics beta-induced Alfvén acoustic eigenmodes modes, are observed in Mirnov coil signals, interferometry, and soft x-ray diagnostics. A moderate amplitude 'primer' chirping mode usually precedes an H–L transition. This is followed by a 'dominant' chirping mode with higher amplitude during the L-mode. The L–H transition back to the improved confinement occurs on a longer time scale of tens of ms, consistent with the slowing down time scale of fast beam ions. A dramatic decrease in toroidal plasma rotation is systematically observed associated with chirping modes sweeping down to zero frequency. Resonance maps built for the beam-driven chirping modes with the ASCOT (accelerated simulation of charged particle orbits in torodoial devices) code show that the resonant beam ions have orbits near the trapped-passing boundary. The ASCOT modelling assesses how losses of the resonant fast ions caused by the chirping modes with high enough amplitude modify the torque, potentially affecting the plasma rotation.

Keywords: fast particle effects in plasma, plasma–beam interactions, spherical tokamak, magnetic confinement fusion, H-mode, chirping modes

(Some figures may appear in colour only in the online journal)

* Author to whom any correspondence should be addressed.

1. Introduction

The quality of plasma confinement is one of the key issues for designing and developing magnetic fusion machines [1]. Transitions from low plasma confinement (L-mode) to high confinement (H-mode) occur when heating power of the plasma exceeds a certain threshold [2]. This power threshold has a parametric dependence predominantly on the toroidal magnetic field, plasma density and plasma boundary surface area [3]. Theory developed for L–H transitions interprets this phenomenon as a result of a dynamical evolution of turbulence and transport in the main thermal plasma species based on the fundamental role of radial electric field E_r and plasma rotation shear suppressing the turbulence [4]. Dithering H-mode has recently been observed and characterised in the high field spherical tokamak ST40 [5]. These H-mode discharges had similar auxiliary heating power and plasma parameters in comparison to L-mode discharges, indicating their proximity to ST40's power threshold. This work presents the novel experimental observation of interplay between the beam driven core-localised modes of sweeping frequency (chirping modes) and quasi-periodic H–L–H transitions in ST40 [6]. The observed interplay is somewhat similar to the high-frequency edge localised mode precursors observed on the Princeton Beta Experiment Modified (PBX-M) tokamak [7], but not on other magnetic fusion devices otherwise. Additional experimental observations of the correlation between chirping modes sweeping down to zero frequency, and the toroidal plasma rotation is also presented. A general criterion has been proposed in the literature that links the emergence of chirping modes with low diffusivity of energetic ions when plasma microturbulence is suppressed and confinement improves [8].

2. Dithering H-mode on ST40

Figure 1 shows a general ST40 dithering H-mode discharge (pulse #9823) with machine and plasma parameters: toroidal field strength $B_T = 2.1$ T; plasma current $I_P = 550$ kA; minor radius $a = 0.27$ m; major radius $R = 0.5$ m; elongation $\kappa = b/a = 1.4$, where b is the vertical axis of the elliptical cross-section of the plasma and neutral beam injection (NBI) power of ∼1 MW for the 55 keV NBI and 0.8 MW for the 25 keV NBI. Both the plasma and beam are deuterium. Figure 1(*d*) shows a reduction in the level of D_α signal as the plasma enters H-mode. Figure 2 shows a zoom of the H–L–H transitions and their correspondence with the chirping modes observed in spectrograms of magnetic measurements. The time interval of the H-mode confinement is also indicated in figure 3, which shows that the spatial gradient of visible light emission changes notably in connection with the period of high D_α signal (figure 2(*c*) 123 ms, figure 3(*a*)) and low D_α signal (figure 2(*c*) 125 ms, figure 3(*b*)). The visible light seen in figure 3(*b*) at low intensity has a much sharper boundary than the light in figure 3(*a*) indicating a sharp plasma

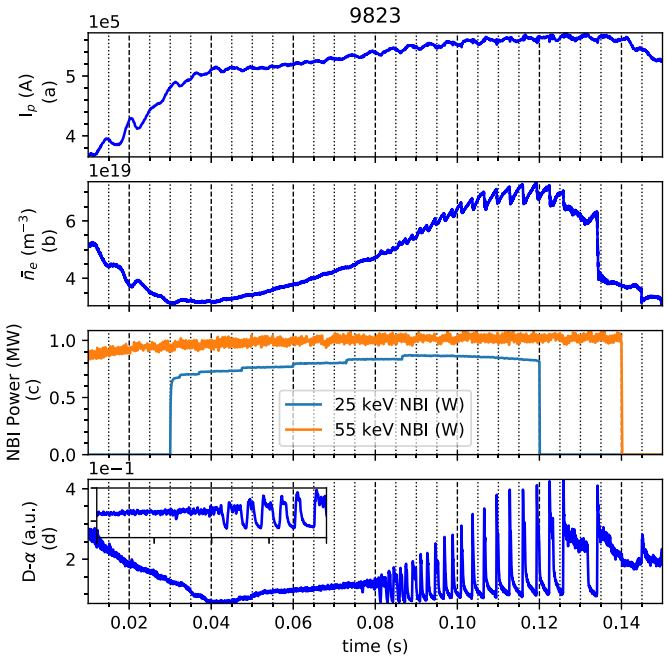

Figure 1. Top to bottom: (*a*) plasma current; (*b*) line averaged density; (*c*) NBI power of the 55 keV and 25 keV beams; (*d*) D_α signal with a zoom of the initial drop in signal from 70 to 90 ms, for pulse 9823.

gradient in figure 3(*b*) typical of the edge transport barrier in H-mode. Currently no edge profile diagnostics are available on ST40 to directly measure the presence of a pedestal. Further characterisation of H-mode observed in ST40 and the L–H transition power threshold are discussed in [5].

3. Interplay of chirping modes with plasma confinement

Figure 2 clearly shows a correlation between chirping modes and the transition between high and low plasma confinement. At the onset of the chirping modes visible in the magnetic signals (figures 1(*b*) and 2(*a*)), transient H–L transitions are observed, with the intensity of D_α signal increasing by a factor of ∼3. Then, the plasma transitions back into H-mode occurs with the D_α signal returning to the previous low levels. When a sequence of the chirping modes occurs at ∼125 ms, the H–L transition causes a longer L-mode dwell period rather than a transient H–L–H event. The chirping modes in figure 2 that correlate with the modulation of the D_α signal are of the sub toroidal Alfvén eigenmode (TAE) frequency range of ∼70–100 kHz. Chirping modes are also present in the much higher TAE frequency range of ∼300–400 kHz, but they occur in L-mode. In what follows we discuss the chirping modes of sub-TAE frequency range only. A zoom in the raw Mirnov coil signal is presented in figure 4, which shows the build-up of small chirping (primer) modes of increasing amplitudes during the H-mode confinement period, followed by a larger (dominant) chirping mode that initiates during the fast

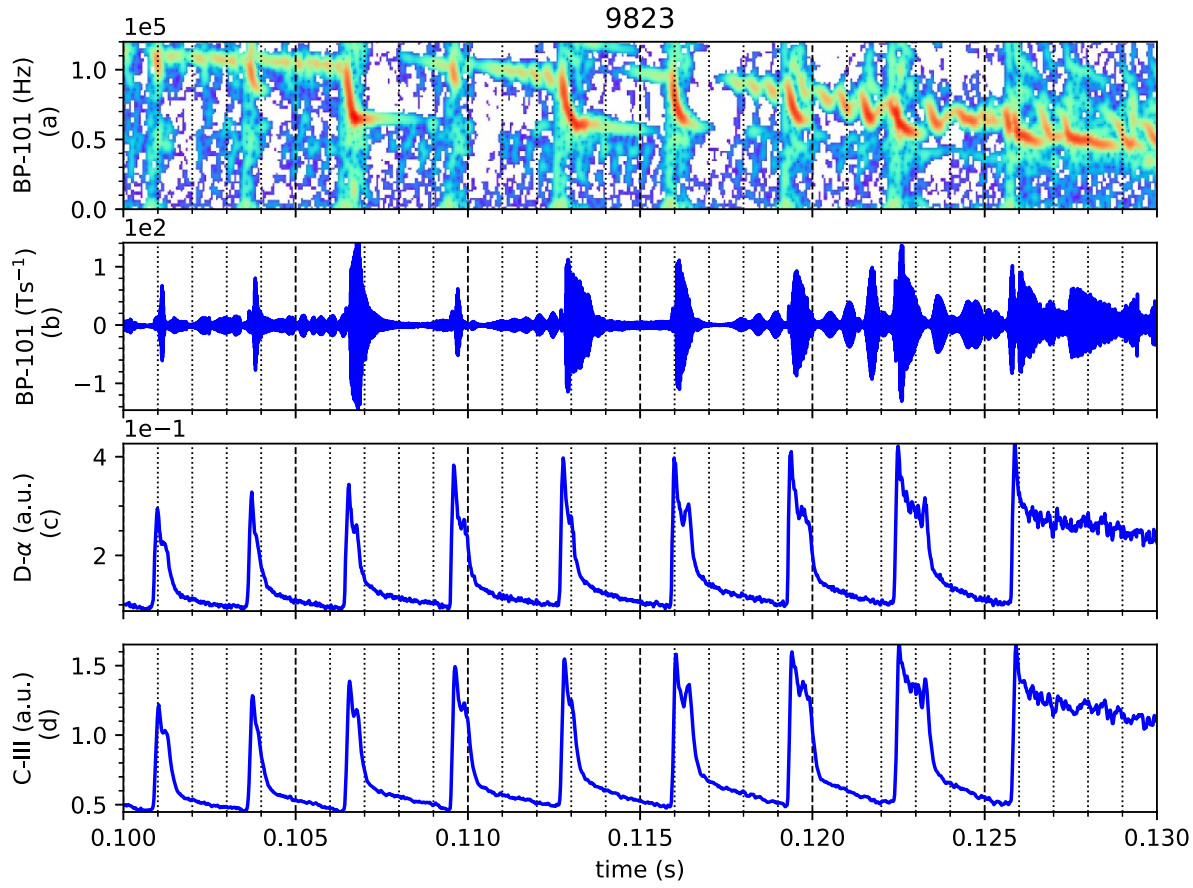

Figure 2. Top to bottom: (*a*) magnetic spectrogram from Mirnov coil showing amplitude (a.u.) and frequency pattern of the chirping modes; (*b*) raw Mirnov coil signal; (*c*) D_α signal; (*d*) C-III signal, with wavelength of 464.7 nm.

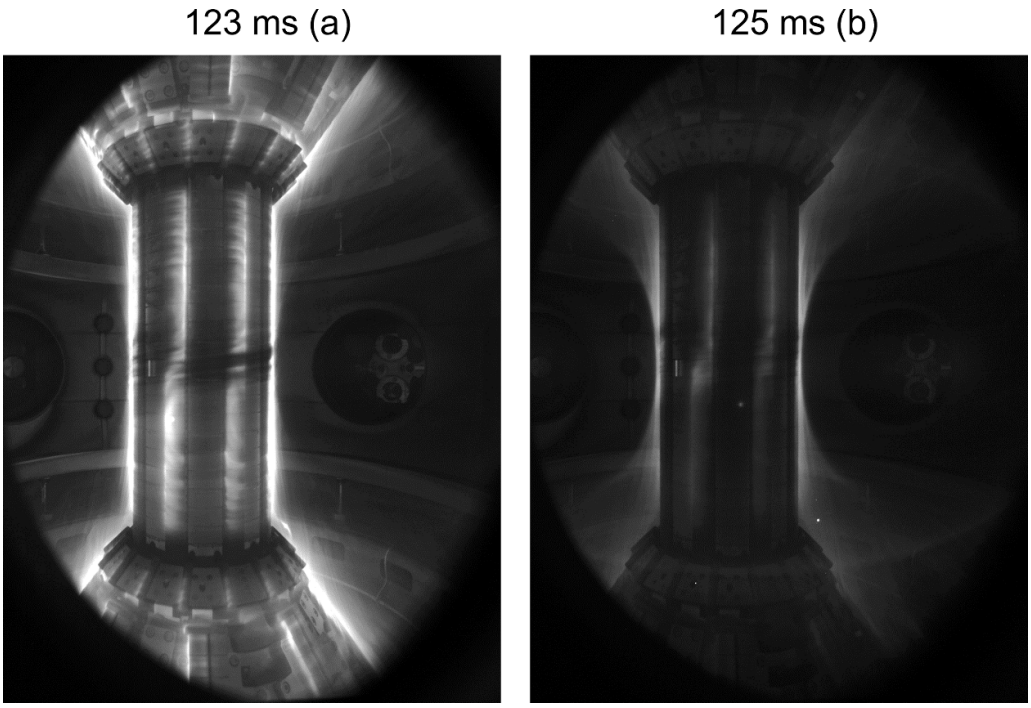

Figure 3. (*a*) Visible light image during L-mode at 123 ms; (*b*) visible light image observed during H-mode at 125 ms; pulse 9823.

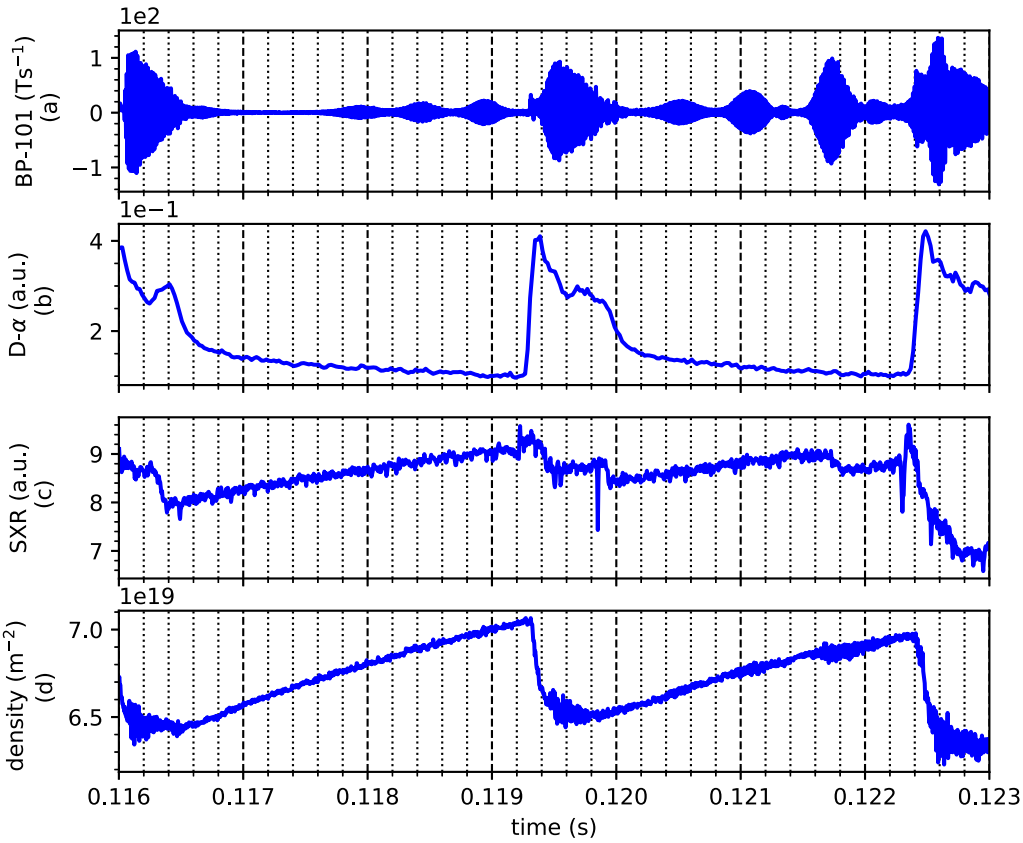

Figure 4. Zoom in for pulse 9823 of: (*a*) the raw Mirnov coil signal; (*b*) the D_α signal (*c*) SXR line-integrated signal for a single chord and (*d*) line-integrated density interferometer. Small chirping modes (primer) of increasing amplitude are observed during the H-mode period, followed by the large amplitude (dominant) mode during the L-mode period.

H–L transition and continues into the L-mode period. This pattern of increasing amplitude primer modes followed by a single dominant mode can be observed for most (but not all) H–L transitions. Aside from the chirping modes, the H–L back-transition correlates with low frequency, sawtooth-like oscillations present in the density interferometer and to a lesser extent the soft x-ray (SXR) signal, as shown in figure 4. The low frequency components of these oscillations are highlighted in the spectrograms shown in figure 6. Figure 4 shows the characteristic timescale of the crash in the SXR signal is around 500 μs, notably longer than the magnetic reconnection time for typical sawtooth oscillations observed on ST40 (100 μs). Usually, sawtooth oscillations are clearly identifiable from the SXR trace, whereas the sawtooth oscillations in figure 4 are weak in intensity and misshaped. On other machines sawtooth oscillations are known to sometimes correlate with L–H transitions, due to the heat transport from the centre to the edge of the plasma caused by the internal kink mode aiding the formation of an edge transport barrier [4, 9]. However, the sawtooth-like oscillations in figure 4 show the opposite trend and correlate with the H–L back transition. These factors call into question the mechanism behind such oscillations, which are referred to as sawtooth-like in this work. Due to the lack on internal profile diagnostics in ST40 we cannot infer whether the sawtooth-like oscillations correspond to the internal kink mode.

4. Plasma rotation and chirping mode correlation

Chirping modes are also observed to systematically correlate with decrease in toroidal plasma rotation in these series of discharges. Due to the limited temporal and intensity resolution of the plasma rotation diagnostic, the decrease in plasma rotation is best observed during the highest amplitude chirping modes where the mode frequency decreases to zero. Figure 5 shows three cases of this type when charge-exchange measurement detected a dramatic decrease of the plasma rotation during large amplitude chirping mode. The chirping mode itself transforms into a lock mode, sweeping down to zero frequency in the end of its evolution. The toroidal plasma velocity is determined using a charge-exchange-recombination-spectroscopy diagnostic measuring the 529 nm spectral line of C^{5+}. Passive and active contributions are fitted to the measured spectra, the ion temperature and toroidal fluid velocity of the C^{6+} impurity ion at the intersection between the 25 keV neutral beam and lines of sight of the diagnostic are estimated from the width and Doppler shift of the active component. The measurement uncertainty comes from the diagonal element of the covariance matrix of a least-square fit (one σ), taking known noise sources into account (analogue-to-digital converters noise, Poisson noise from detected photoelectrons). Clearly present in figure 5 is a lower amplitude mode around 50 kHz, which is also present in the beta-induced Alfvén

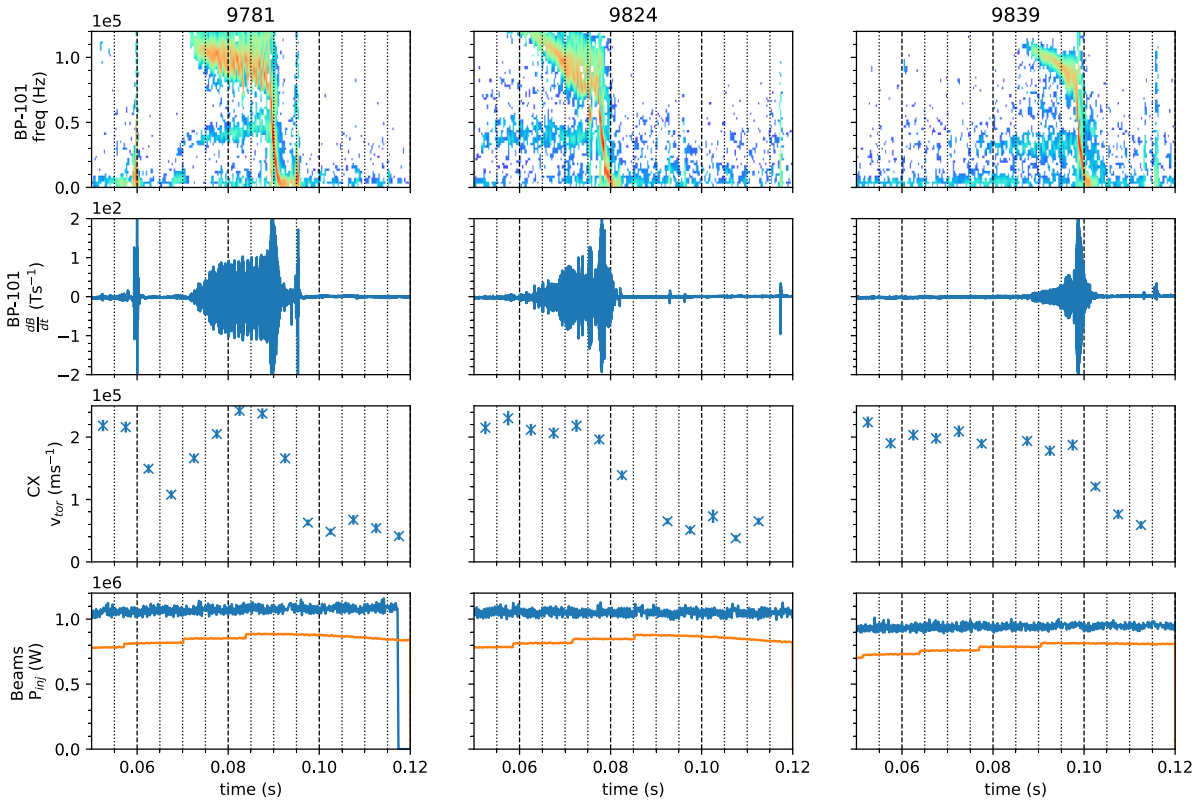

Figure 5. Top to bottom: magnetic spectrogram showing amplitude and frequency pattern of the chirping modes; raw Mirnov coil signal; toroidal plasma rotation measured at a major radius of 0.44 m with the line integrated charge-exchange diagnostic ($r/a \sim 0.22$); injected beam power of the two beams.

acoustic eigenmode (BAAE) gap according to calculations due to the broad gap width $\Delta\omega = (2v_A/Rq)\,\delta\sqrt{1+2q^2}$, where v_A is the Alfvén velocity, R is the major radius, q is the safety factor and $\delta \equiv \gamma\beta/2$ is a parameter dependent on the specific heat ratio γ and the plasma beta [10]. The subdominant mode is narrower and is located closer to the plasma centre with a smaller gradient.

Figure 6 shows the presence of chirping modes in sub-millimetre interferometer and SXR signals, in addition to the magnetic perturbation signal. The SXR system consists of 20 chords that form a fan in the vertical plane. As the presence of chirping modes is limited to chords that passed through the plasma centre, we conclude that the chirping modes are localised deeply in the plasma core. The multiple modes that are stacked above one another in frequency space at 135 ms resembles an Alfven avalanche as described in [11].

5. Modelling and discussion

Modelling performed with the NOVA (nonvariational ideal MHD stability) code suggests these electromagnetic modes of sub-TAE frequency range are BAAE-modes [12], with radial mode structure similar to that obtained from the internal plasma measurements. For a fixed toroidal mode number $n = 1$, the mode was comprised of a variety of poloidal harmonics, with $m = 1$ having the largest amplitude (as shown in figure 7). To assess the resonant beam-mode interaction and losses of energetic beam ions, the initial value particle-following ASCOT code [13] has been used. The simulations on the beam ion evolution were performed with an imposed core-localised $n = 1$, $m = 1$ magnetohydrodynamics (MHD) mode (figure 7) as identified by simulations with the NOVA MHD spectral code [14, 15]. The resultant resonance maps between the beam drift orbits and a discrete frequency mode (f_{mode}) show how particle orbits of a given energy and pitch angle interact strongly with the specified mode in resonance. Figure 8(a) shows the overlaid resonant maps for 70, 80 and 90 kHz mode frequencies, with a colour scale corresponding to the resonance condition expressed as $-\log\left(f_{\mathrm{mode}} - n \times f_{b,\mathrm{tor}} - p \times f_{b,\mathrm{pol}}\right)$, where $f_{b,\mathrm{tor}}$ and $f_{b,\mathrm{pol}}$ are the frequencies of the beam drift orbits in the toroidal and poloidal direction respectively, n is the toroidal mode number, and p is an integer. The frequencies were calculated from the toroidal and poloidal orbit times for markers launched at the mode location $\rho_{\mathrm{pol}} = 0.2$, where $\rho_{\mathrm{pol}} = \sqrt{(\psi_\theta - \psi_{\theta,\mathrm{axis}})/(\psi_{\theta,\mathrm{sep}} - \psi_{\theta,\mathrm{axis}})}$. The high intensity resonance lines shown in figure 8(a) have a very sharp gradient with respect to the pitch-angle but are almost constant as functions of the beam energy. The high energy resonance orbits circled in figure 8(a) show the fast particle beam population that interacts with the mode. The types of the orbits resonating with the chirping modes are mostly those from the trapped-passing boundary (pitch angle $\frac{v_\parallel}{v}$ between -0.5 and -0.6) as figure 8(b) shows. The resonance preference of

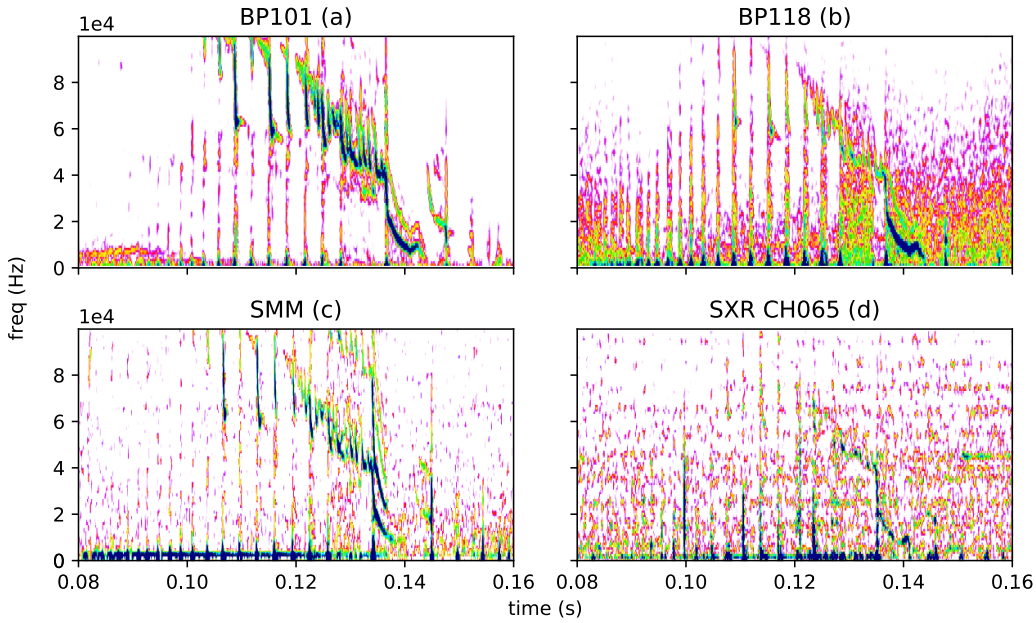

Figure 6. A set of chirping modes from pulse 9823 seen simultaneously in: (*a*) magnetic signal ($\delta B = \frac{dB}{dt}/\omega$) from an outboard Mirnov coil; (*b*) magnetic signal ($\delta B = \frac{dB}{dt}/\omega$) from an inboard Mirnov coil; (*c*) line-integrated density interferometry signal; (*d*) SXR line-integrated signal for a single chord, orientated with an angle of $\sim$0.45° above mid-plane in the *RZ* plane (i.e. directed through the core of the plasma).

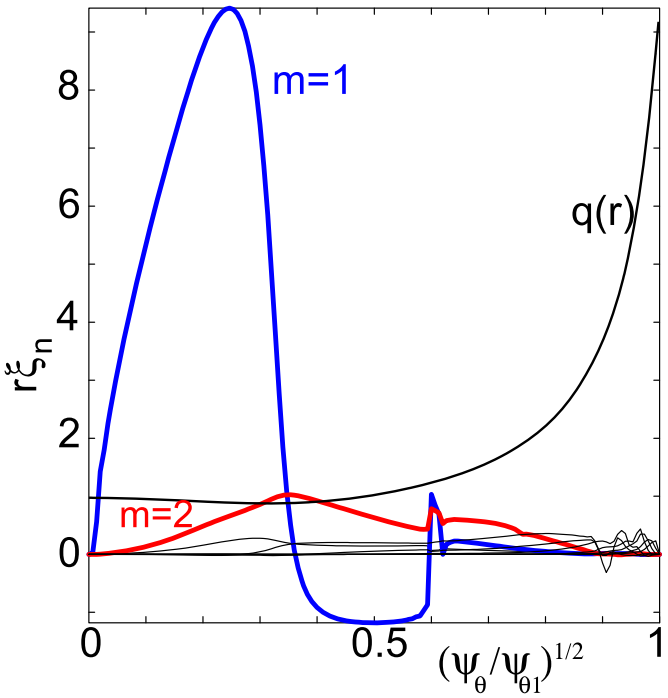

Figure 7. The radial structure of BAAE poloidal harmonics of the normal component of the plasma displacement (ε_n) in arbitrary units vs the square root of the poloidal magnetic flux (ψ_θ) normalised. The mode structure is computed for the pulse 9781, at 8 ms. Also shown is the radial dependence of the safety factor, q as noted in the figure.

trapped particle orbits over passing orbits is due to the reduced poloidal and toroidal frequency of the trapped particle orbits, which lies closer to the mode frequency of interest. Note that the resonance curves go from the low energy thermal ions at $\left|v_\parallel/v\right| < 0.5$ to the high energy beam ions.

Figure 9(*a*) demonstrates the reduced fast particle content in the region $\rho < 0.2$ and corresponding reduction in the NBI torque. As the plasma's toroidal velocity prior to the mode is relatively fixed, the accelerating beam torque is matched by the opposing viscous torque, hence a reduction in beam torque would lead to a corresponding reduction in the plasma rotation, as observed in figure 5. The reduction in toroidal plasma velocity by the modelled chirping modes could boost the turbulence and weaken the edge transport barrier of a H-mode plasma, leading to the plasma transitioning into L-mode. This provides a plausible explanation for the observed

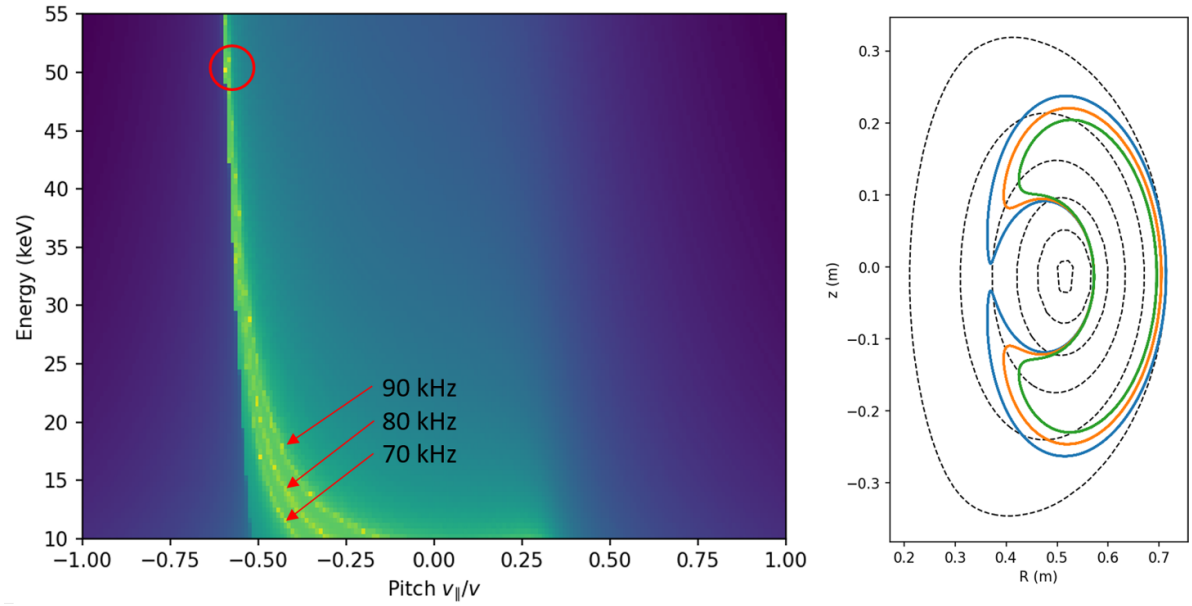

Figure 8. (*a*) The left plot shows three resonance maps of the beam ions interacting with the chirping modes for overlaid mode frequencies of 70, 80 and 90 kHz. The resonance condition is expressed as $-\log\left(f_{\text{mode}} - n \times f_{\text{beam,tor}} - p \times f_{\text{beam,pol}}\right)$. Pitch is defined as $v_\parallel/v$; (*b*) the right plot shows drift orbits corresponding to ions launched at 50 keV and pitch-angles highlighted with red circle in (*a*).

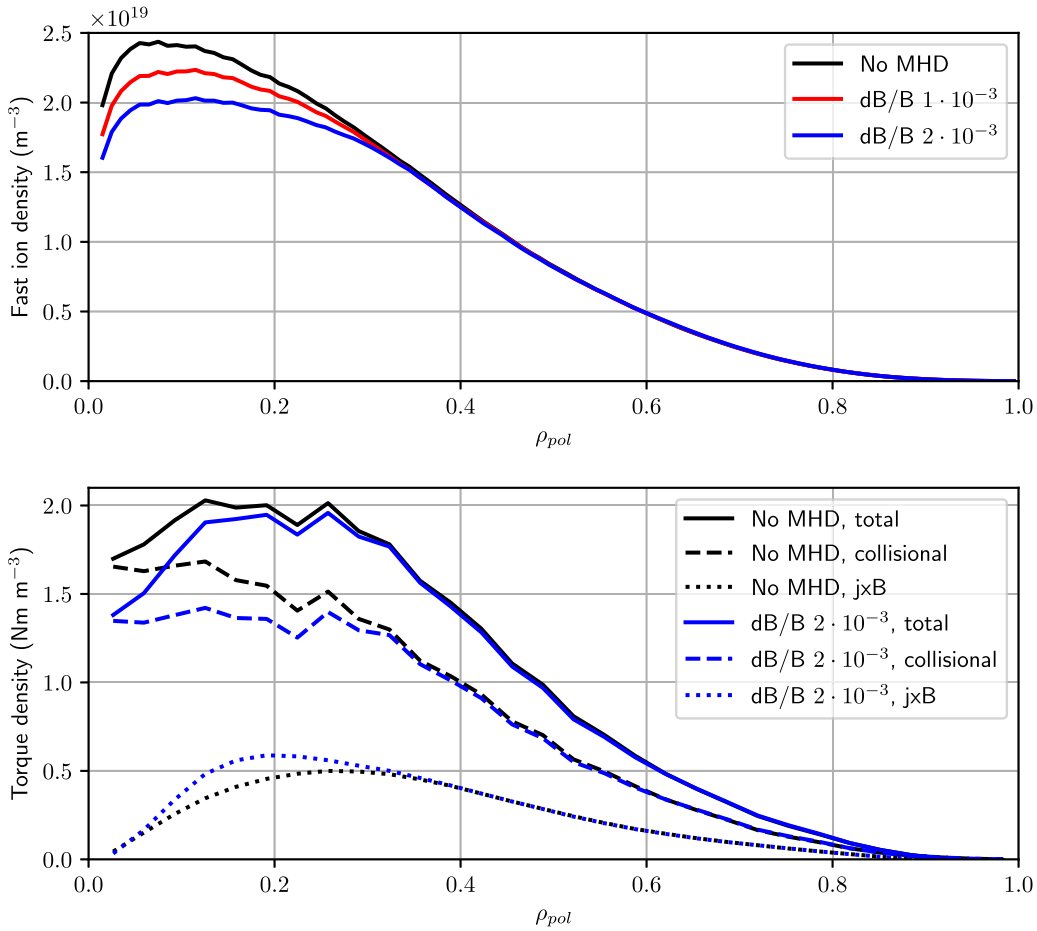

Figure 9. (*a*) The top plot shows the MHD mode at 90 kHz with varying amplitudes impacts the radial profile of fast ion density. (*b*) The bottom plot shows the radial profile of the beam's torque density, split into collisional (momentum loss due to premature loss of fast ions) and $J \times B$ (particle drift or losses leading to a radial current that interacts with the poloidal B field) components, for both with and without the MHD mode.

interplay between chirping modes and H–L–H mode transitions as observed in figure 2. The pulse's proximity to the L–H power threshold also limits the size of perturbation needed, for the plasma to transition. Figure 9(*b*) divides the beam torque into its collisional and $J \times B$ components. This shows that the collisional torque is most strongly affected by the presence of the chirping mode, leading to the reduction in the net torque.

6. Conclusion

In summary, this letter presents the experimental correlation between chirping modes and the plasma's transition from high to low confinement. Primer chirping modes are observed during the H-mode period, followed by a dominant chirping mode during L-mode. Further work is required to validate the preliminary theoretical explanations through additional fast particle simulations and integrated modelling simulations that incorporate beam torque to accurately determine its impact on plasma rotation, turbulence, and confinement.

Acknowledgments

We would like to thank Y. Andrew for useful discussions, in particular on H-mode confinement and M. Sertoli for discussion and description of the charge-exchange measurements. The work of S.E.S. has been part-funded by the EPSRC Energy Programme (Grant No. EP/W006839/1).

ORCID iDs

J. Bland https://orcid.org/0000-0002-4083-7812
S.E. Sharapov https://orcid.org/0000-0001-7006-4876

References

[1] ITER Physics Expert Group on Energetic Particles, Heating and Current Drive and ITER Physics Basis Editors 1999 Chapter 5: physics of energetic ions *Nucl. Fusion* **39** 2471
[2] Wagner F. *et al* 1982 Regime of improved confinement and high beta in neutral-beam-heated divertor discharges of the ASDEX tokamak *Phys. Rev. Lett.* **49** 1408
[3] Andrew Y., Bähner J.-P., Battle R. and Jirman T. 2019 H-mode power threshold studies on MAST *Plasma* **2** 328
[4] Wagner F. 2007 A quarter-century of H-mode studies *Plasma Phys. Control. Fusion* **49** B1
[5] Andrew Y., Bland J., Buxton P., Dnestrovskij A., Gryaznevich M.P., Romanelli M., Sertoli M., Thomas P. and Varje J. H-mode dithering phase studies on ST40 *Phil. Trans.* A submitted
[6] Gryaznevich M.P. *et al* 2022 Experiments on ST40 at high magnetic field *Nucl. Fusion* **62** 042008
[7] Kaye S.M. *et al* 1990 Characteristics of high frequency ELM precursors and edge stability in the PBX-M tokamak *Nucl. Fusion* **30** 2621
[8] Duarte V.N., Berk H.L., Gorelenkov N.N., Heidbrink W.W., Kramer G.J., Nazikian R., Pace D.C., Podestà M., Tobias B.J. and van Zeeland M.A. 2017 Prediction of nonlinear evolution character of energetic-particle-driven instabilities *Nucl. Fusion* **57** 054001
[9] Martin Y.R. TCV Team 2004 Synchronization of L-mode to H-mode transitions on the sawtooth cycle in ohmic TCV plasmas *Plasma Phys. Control. Fusion* **46** A77
[10] Gorelenkov N.N. *et al* 2007 Predictions and observations of global beta-induced Alfvén—acoustic modes in JET and NSTX *Plasma Phys. Control. Fusion* **49** B371
[11] Fredrickson E.D., Gorelenkov N.N., Bell R.E., Menard J.E., Roquemore A.L., Kubota S., Crocker N.A. and Peebles W. 2006 Fast ion loss in a 'Sea-of-TAE' *Nucl. Fusion* **46** S926
[12] Gorelenkov N.N., Berk H.L., Fredrickson E. and Sharapov S.E. JET EFDA Contributors 2007 Predictions and observations of low-shear beta-induced shear Alfvén–acoustic eigenmodes in toroidal plasmas *Phys. Lett.* A **370** 70
[13] Varje J., Särkimäki K., Kontula J., Ollus P., Kurki-Suonio T., Snicker A., Hirvijoki E. and Äkäslompolo S., 2019 High-performance orbit-following code ASCOT5 for Monte Carlo simulations in fusion plasmas (arXiv:1908.02482)
[14] Cheng C.Z. and Chance M.S. 1986 Low-n shear Alfvén spectra in axisymmetric toroidal *Plasmas Phys. Fluids* **29** 8
[15] Gorelenkov N.N., Van Zeeland M.A., Berk H.L., Crocker N.A., Darrow D., Fredrickson E., Fu G.-Y., Heidbrink W.W., Menard J. and Nazikian R. 2009 Beta-induced Alfvén-acoustic eigenmodes in national spherical torus experiment and DIII-D driven by beam ions *Phys. Plasmas* **16** 056107